AIP | Journal of Applied Physics

Photo-electromotive-force from volume speckle pattern vibration with large amplitude

T. O. dos Santos, J. C. Launay, and J. Frejlich

Citation: J. Appl. Phys. **103**, 113104 (2008); doi: 10.1063/1.2938061
View online: http://dx.doi.org/10.1063/1.2938061
View Table of Contents: http://jap.aip.org/resource/1/JAPIAU/v103/i11
Published by the AIP Publishing LLC.

Photo-electromotive-force from volume speckle pattern vibration with large amplitude

T. O. dos Santos,[1] J. C. Launay,[2] and J. Frejlich[1,a)]
[1]*Instituto de Física "Gleb-Wataghin," UNICAMP, 13083-970 Campinas, São Paulo, Brazil*
[2]*ICMCB, CNRS, Université Bordeaux 1, 33608 Pessac Cedex, France*

(Received 15 November 2007; accepted 7 April 2008; published online 5 June 2008)

We report an accurate mathematical model describing the photo-electromotive-force signal produced by a speckle pattern of light vibrating in the volume of a photorefractive crystal with a large transverse amplitude. Our model shows that, for vibrations much faster than the material response time, the first harmonic term of the photo-electromotive-force signal exhibits a maximum at a characteristic value of the vibration-amplitude-to-speckle-size ratio that depends on the dark-to-photoconductivity ratio in the material. The theoretical results are in good agreement with experimental data from a vanadium-doped photorefractive CdTe (CdTe:V) crystal under 1064 nm wavelength illumination. © *2008 American Institute of Physics*. [DOI: 10.1063/1.2938061]

I. INTRODUCTION

A photo-electromotive-force (photo-emf) signal is produced in photorefractive or simply photoconductive[1,2] materials by the vibration of a spatial pattern of light. The light excites electrons (and/or holes) that vibrate along with the pattern of light in the conduction band (or valence band for holes) and, for sufficiently slow response materials, a stationary spatial distribution of charges (and associated space-charge field) is also produced in the material volume. The vibration of the photoexcited charge carriers in the stationary space-charge field produces an electromotive force (photo-emf) with the same frequency of the pattern of light. This photo-emf may be used to measure the vibration amplitude of the target producing this pattern of light.

The first experimental results involving photo-emf in photorefractive materials were published in 1986.[3] Since then this technique became very popular mainly for the measurement of mechanical vibrations.[4–7] Photo-emf signals can be produced either by a holographic[1,3,8] or a speckle[4] pattern of light, each one of them having specific features and practical applications.[9,10] A comprehensive review on this subject was published by Stepanov.[6] The first experimental results were focused on small vibration amplitudes,[1,11] in which case the amplitudes and the resulting photo-emf signals are lineraly proportional. The theory was generalized for large amplitude holographic pattern vibrations[5] and for the case of strongly absorbing materials[12] as well as for the case of speckle patterns.[13]

Many photorefractive and photoconductive materials have already been successfully used as active media for speckle photo-emf experiments and associated applications, including $Bi_{12}SiO_{20}$,[1,3,5] $Bi_{12}TiO_{20}$,[2,8,13] GaAs,[4,14–16] CdTe,[10,17–19] and even organic photoconductors,[20] among many others.

In the present paper, we report a general comprehensive theoretical development and a detailed analysis of volume speckle-based photo-emf and show that a maximum in the first temporal harmonic component of the photo-emf signal does actually occur at a fixed vibration-amplitude-to-speckle-size ratio close to $\delta=0.9$. These values are somewhat higher than the one already reported before[13] using a rather simplified theoretical model. Preliminary experimental results using a CdTe:V crystal under $\lambda=1064$ nm speckle pattern illumination are in good agreement with the present theoretical development.

II. THEORY

The speckle pattern irradiance is currently assumed to be originated by the diffraction of scattered light through an aperture (usually circular, of diameter Φ) and observed at a distance f. It is therefore represented by randomly distributed Airy functions in the sample volume, where the first Airy minimum is[21]

$$R_0 = 1.22\frac{f}{\Phi}\lambda \tag{1}$$

and represents the speckle radius, with λ being the light wavelength. It is possible to show that the Airy function can be closely approximated by the Gaussian function

$$I = I_0 e^{-r^2} \quad \text{with } r^2 \equiv x^2 + y^2, \tag{2}$$

$$x^2 \equiv (X/W)^2 \quad \text{and} \quad y^2 \equiv (Y/W)^2, \tag{3}$$

where $W \equiv R_0/2$, with X and Y being the spatial coordinates and x and y the reduced coordinates. The use of a Gaussian instead of an Airy function strongly facilitates calculations, but is limited to $\sqrt{x^2+y^2} \leq 2$ only. Following Ref.22, we shall assume that electrons are the predominant charge carriers in CdTe:V for the 1064 nm wavelength illumination in this paper. In this case, the rate equations relating the free electron density $\mathcal{N}$ in the conduction band and the total (N_D) and the empty (N_D^+) electron donor densities are[23,24]

$$\frac{\partial N_D^+}{\partial t} = G - R, \tag{4}$$

a)Electronic mail: frejlich@ifi.unicamp.br.

$$G \equiv (N_D - N_D^+)\left(\frac{sI}{h\nu} + \beta\right), \tag{5}$$

$$R \equiv \gamma N_D^+ \mathcal{N}/\tau \quad \text{with } 1/\tau = \gamma N_D^+, \tag{6}$$

where s is the effective donor cross section for electron generation by light with photonic energy $h\nu$, β is the dark electronic generation, γ is the recombination parameter, and τ is the photoelectron lifetime.

A. Stationary conditions

In stationary conditions, for a time scale much larger than the characteristic material recording (space-charge buildup) time τ_{sc} and for $\tau_{sc} \gg \tau$, we have

$$\frac{\partial N_D^+}{\partial t} = 0 \tag{7}$$

that, when substituted into Eqs. (4)–(6), leads to

$$\mathcal{N} = \mathcal{N}_0 e^{-r^2} + \mathcal{N}_d, \tag{8}$$

$$\text{with } \mathcal{N}_0 \equiv (N_D - N_D^+)\frac{sI_0}{h\nu}\tau \tag{9}$$

$$\text{and } \mathcal{N}_d \equiv \beta\tau, \tag{10}$$

where $\mathcal{N}_0$ is the term associated with I_0, and $\mathcal{N}_d$ is the value in the dark. The photogenerated current density is therefore

$$\mathbf{j} = q\mu\mathcal{N}\mathbf{E} + qD\nabla\mathcal{N}, \tag{11}$$

$$\nabla\mathcal{N} = -2\frac{\mathcal{N}_0}{W}(\hat{\mathbf{x}}x + \hat{\mathbf{y}}y)e^{-r^2}, \tag{12}$$

where μ and D are the mobility and diffusion coefficients of the charge carriers, q is the value of the electric charge of the electron, and $\hat{\mathbf{x}}$ and $\hat{\mathbf{y}}$ are the corresponding unit vectors. A space-charge electric field arises, where the x and y components are computed from Eq. (11) and are respectively

$$E_x = \frac{E_0 + 2E_D x e^{-r^2}}{e^{-r^2} + R_d}, \tag{13}$$

$$E_y = \frac{2E_D y e^{-r^2}}{e^{-r^2} + R_d}, \tag{14}$$

where E_0 is the external electric field applied between both electrodes, along the coordinate x, with

$$E_0 \equiv \frac{j_0}{q\mu\mathcal{N}_0}, \tag{15}$$

$$E_D \equiv \frac{D}{W\mu}, \tag{16}$$

$$R_d \equiv \mathcal{N}_d/\mathcal{N}_0, \tag{17}$$

where j_0 is the average current density along direction $\hat{\mathbf{x}}$.

B. Vibrating pattern of light

For the case wherein the pattern of light is vibrating along coordinate x with reduced amplitude δ and angular frequency Ω, the expressions in Eqs. (2) and (8) become

$$I = I_0 e^{-(r^2+\delta^2/2)} I_1(x,\delta,\Omega,t), \tag{18}$$

$$\mathcal{N} = \mathcal{N}_0 e^{-(r^2+\delta^2/2)} I_1(x,\delta,\Omega,t) + \mathcal{N}_d, \tag{19}$$

with

$$I_1(x,\delta,\Omega,t) \equiv e^{-2x\delta \sin \Omega t} + (\delta^2/2)\cos 2\Omega t. \tag{20}$$

From Eq. (11), the photocurrent density components along coordinates x and y are respectively computed as

$$j_x = q\mu\mathcal{N}E_x + qD(\nabla\mathcal{N})_x, \tag{21}$$

$$j_y = q\mu\mathcal{N}E_y + qD(\nabla\mathcal{N})_y, \tag{22}$$

with

$$(\nabla\mathcal{N})_x = -2[xI_1(x,\delta,\Omega,t) + \delta I_2(x,\delta,\Omega,t)]\frac{\mathcal{N}_0}{W}e^{-(r^2+\delta^2/2)}, \tag{23}$$

$$(\nabla\mathcal{N})_y = -2yI_1(x,\delta,\Omega,t)\frac{\mathcal{N}_0}{W}e^{-(r^2+\delta^2/2)}, \tag{24}$$

$$I_2(x,\delta,\Omega,t) \equiv I_1(x,\delta,\Omega,t)\sin \Omega t. \tag{25}$$

Assuming that τ_{sc} is much larger than the period $1/\Omega$ of the vibrating pattern ($\Omega\tau_{sc} \gg 1$) and the latter, in turn, is much larger than the photoelectron lifetime τ ($\Omega\tau \ll 1$), the time-average photocurrent value along x and y are respectively

$$j_0 = \langle j_x \rangle = q\mu\langle\mathcal{N}\rangle E_x + qD\langle(\nabla\mathcal{N})_x\rangle, \tag{26}$$

$$0 = \langle j_y \rangle = q\mu\langle\mathcal{N}\rangle E_y + qD\langle(\nabla\mathcal{N})_y\rangle, \tag{27}$$

with

$$\langle\mathcal{N}\rangle = N_0 e^{-(r^2+\delta^2/2)} I_{1M}(x,\delta,\Omega) + \mathcal{N}_d, \tag{28}$$

$$\langle(\nabla\mathcal{N})_x\rangle = -2\frac{\mathcal{N}_0}{W}e^{-(r^2+\delta^2/2)}[xI_{1M}(x,\delta,\Omega) + \delta I_{2M}(x,\delta,\Omega)], \tag{29}$$

$$\langle(\nabla\mathcal{N})_y\rangle = -2\frac{\mathcal{N}_0}{W}e^{-(r^2+\delta^2/2)} yI_{1M}(x,\delta,\Omega), \tag{30}$$

where $\langle\ \rangle$ represents the time average and

$$I_{1M}(x,\delta,\Omega) \equiv \langle I_1(x,\delta,\Omega,t)\rangle = \frac{\Omega}{2\pi}\int_{-2\pi/\Omega}^{2\pi/\Omega} I_1(x,\delta,\Omega,t)dt, \tag{31}$$

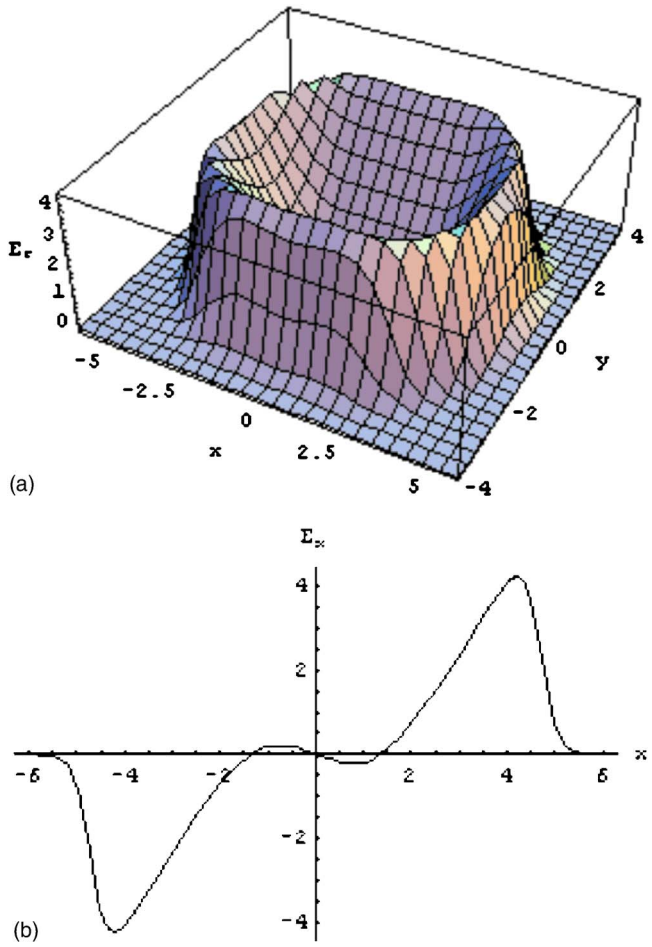

FIG. 1. (Color online) Computed space-charge field modulus E_r (in kV/m) in the x-y plane (top) and E_x component vs x at $y=0$ (bottom) oscillating along coordinate x with $\delta=2$, $E_0=0$, $E_D=1000$ V/m, $\Omega=10$ Hz, $j_D=1$ A/m^2, and $R_d=0.0001$.

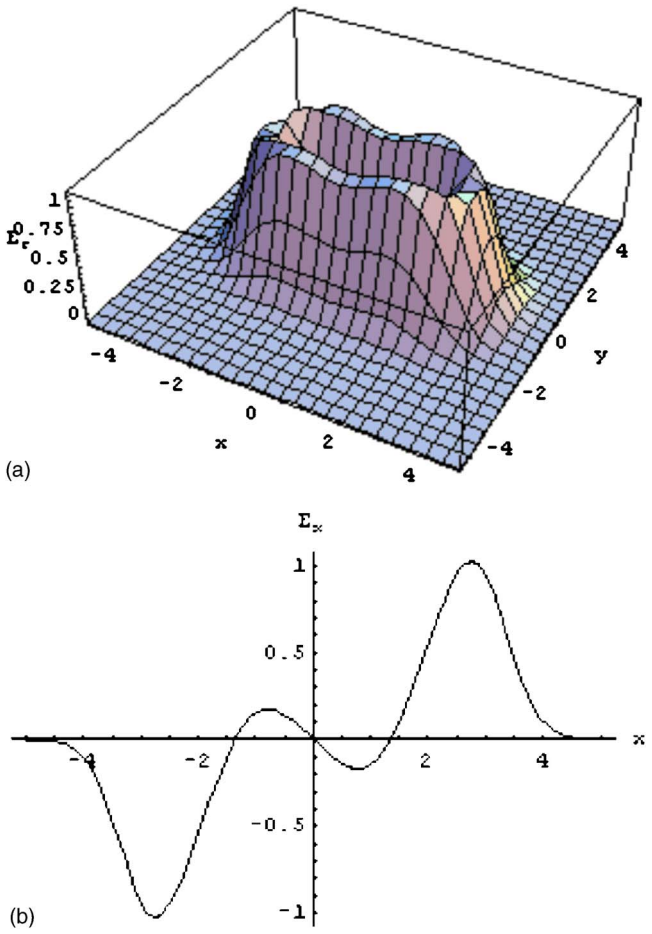

FIG. 2. (Color online) E_r (in kV/m) in the x-y plane (top) and E_x vs x at $y=0$ (bottom) with all parameters as in Fig. 1 but $R_d=0.1$.

$$I_{2M}(x,\delta,\Omega) \equiv \langle I_2(x,\delta,\Omega,t)\rangle = \frac{\Omega}{2\pi}\int_{-2\pi/\Omega}^{2\pi/\Omega} I_2(x,\delta,\Omega,t)dt. \tag{32}$$

From Eqs. (26) and (27), we computed the x and y components as well as the absolute vector modulus of the stationary space-charge field, which are respectively

$$E_x = \frac{E_0}{e^{-(r^2+\delta^2/2)}I_{1M}(x,\delta,\Omega)+R_d} + 2E_D e^{-(r^2+\delta^2/2)}\frac{xI_{1M}(x,\delta,\Omega)+\delta I_{2M}(x,\delta,\Omega)}{e^{-(r^2+\delta^2/2)}I_{1M}(x,\delta,\Omega)+R_d}, \tag{33}$$

$$E_y = 2E_D e^{-(r^2+\delta^2/2)}\frac{yI_{1M}(x,\delta,\Omega)}{e^{-(r^2+\delta^2/2)}I_{1M}(x,\delta,\Omega)+R_d}, \tag{34}$$

$$E_r = \sqrt{E_x^2+E_y^2}. \tag{35}$$

Figures 1 and 2 show the theoretically computed modulus E_r and component E_x for $\delta=2$ with identical experimental parameters, but with different values of the dark-to-bright conductivity parameter R_d. From these figures, it becomes clear that it is not possible to neglect the dark conductivity because it has a large effect on space-charge field shaping.

The x-component current density averaged along the interelectrode distance L along coordinate x is calculated by substituting Eq. (33) into Eq. (21) and accounting for

$$\frac{1}{\ell}\int_{-\ell/2}^{\ell/2} qD(\nabla\mathcal{N})_x dx = 0, \tag{36}$$

which leads to

$$\bar{j}_x(t) = \frac{1}{\ell}\int_{-\ell/2}^{\ell/2} q\mu\mathcal{N}E_x dx, \tag{37}$$

with $\ell \equiv L/W \gg 1$. The time-independent term is

$$\bar{j}_{x0} = j_D R_d \frac{1}{\ell}\int_{-\ell/e}^{\ell/2} \frac{(E_0/E_D)+2e^{-(r^2+\delta^2/2)}[xI_{1M}(x,\delta,\Omega)+\delta I_{2M}(x,\delta,\Omega)]}{e^{-(r^2+\delta^2/2)}I_{1M}(x,\delta,\Omega)+R_d}dx, \tag{38}$$

$$j_D \equiv q\mu\mathcal{N}_0 E_D, \tag{39}$$

which, because of the symmetry properties of I_{1M} and I_{2M} along coordinate x, simplifies to

$$j_{x0} = j_D R_d \frac{E_0}{E_D}\frac{1}{\ell}\int_{-\ell/2}^{\ell/2}\frac{1}{e^{-(r^2+\delta^2/2)}I_{1\mathrm{M}}(x,\delta,\Omega)+R_d}dx. \tag{40}$$

The time-dependent term is similarly calculated as

$$\bar{j}_{xt}(t) = \frac{j_D}{\ell}\int_{-\ell/2}^{\ell/2}\frac{[(E_0/E_D)+2e^{-(r^2+\delta^2/2)}(xI_{1\mathrm{M}}+\delta I_{2\mathrm{M}})]e^{-(r^2+\delta^2/2)}}{e^{-(r^2+\delta^2/2)}I_{1\mathrm{M}}(x,\delta,\Omega)+R_d}I_1(x,\delta,\Omega,t)dx. \tag{41}$$

The function $\bar{j}_{xt}(t)$ is periodic in Ω so that it can be written as a Fourier series as follows:

$$\bar{j}_{xt}(t) = \frac{a_0}{2} + \sum_{N=0}^{N=\infty}(a_N \cos N\Omega t + b_N \sin N\Omega t), \tag{42}$$

where

$$a_N = \frac{\Omega}{\pi}\int_0^{2\pi/\Omega}\bar{j}_{xt}(t)\cos N\Omega t dt, \tag{43}$$

$$b_N = \frac{\Omega}{\pi}\int_0^{2\pi/\Omega}\bar{j}_{xt}(t)\sin N\Omega t dt. \tag{44}$$

It is possible to show that $a_1 \approx 0$, but b_1 instead is not null. The parameter b_1 was plotted (with arbitrarily fixed $j_D=1$) as a function of the reduced vibration amplitude δ in Fig. 3 and shows a maximum varying from $\delta \approx 0.85$ for $R_d=0.1$ to $\delta \approx 0.9$ for $R_d=0$. The calculations above are for $y=0$. As y shifts away from zero, the maximum of b_1 decreases (as expected from the three-dimensional plots in Figs. 1 and 2) but its position is independent of y. As we are mainly interested in the position of the maximum, we restricted our calculations to $y=0$.

The development above assumes the linear addition of speckle signals in the sample volume that is reasonable for our relatively low intensity pattern of light to produce a linearized space-charge field modulation without cross-talking effects. We also assume the synchronized addition of signals from the speckles because they are all coherently driven by the movement of a single speckle pattern of light.

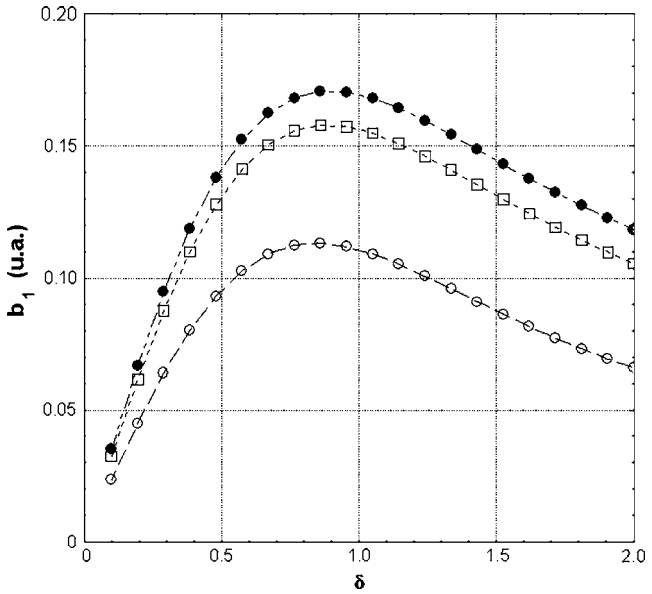

FIG. 3. Plot of b_1 (arbitrary units) as a function of δ for $y=0$, $E_D=1000$ V/m, $j_D=1$, $E_0=0$, and different values of $R_d=0$ (●), 0.01 (□), and 0.1 (○).

III. EXPERIMENT

The theoretical development above was experimentally verified in the setup schematically represented in Fig. 4 using a vanadium-doped photorefractive CdTe crystal (CdTe:V labeled BR4ZM1/b with 5×10^{17} cm^{-3} concentration of V) produced in the ICMCB, France, with thickness $d=2.6$ mm, height $H=9.39$ mm, and interelectrode distance $L=4.2$ mm. This crystal was grown in a four-zone oven and annealed in Ar/H_2 gas mixture at 200 °C to remove the oxygen on its surface and relieve stresses. The electrodes are conductive silver glue applied on the lateral crystal surfaces transverse to the direction of light through the sample. The vibrating target is a small and thin diffusing glass plate ground polished on both faces and firmly glued to the cone of a commercial loudspeaker. The latter is driven by a signal genera-

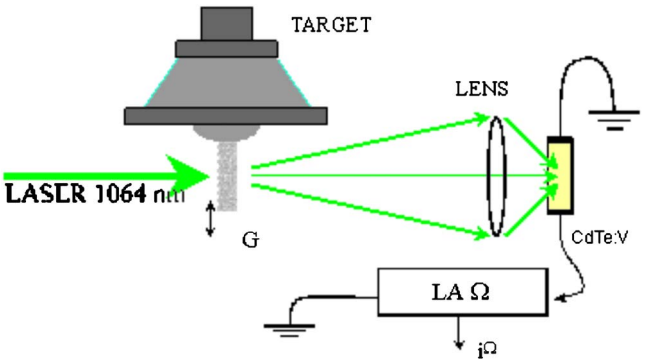

FIG. 4. (Color online) Schematical experimental setup: the target is a diffusing glass plate **G** fixed to the cone of a commercial loudspeaker; the target is illuminated by a 1064 nm wavelength direct laser beam. The scattered light through the target is collected by a lens and focused onto the crystal CdTe:V. The photocurrent is collected by lateral electrodes on the crystal and fed to a lock-in amplifier LAΩ, where the output is the first harmonic i^{Ω} of the photocurrent.

tor and by this means the target is moved (as shown by the small arrow direction) with controlled amplitude and frequency. A laser (low power He–Ne 633 nm wavelength) Doppler vibrometer setup is used to independently measure the target movement. The direct 1064 nm wavelength beam from a Nd:YAG laser (ADLAS—now COHERENT—model 300, 350 mW cw) is directed perpendicularly onto the glass plate target and the scattered light through the target is collected by a commercial photographic objective lens and focused onto the CdTe:V crystal. The first harmonic photo-emf component i^{Ω} is measured using a dual-phase Ω-tuned lock-in amplifier (Signal Recovery model 5210, which is able to operate in current as well as in voltage measurement mode). The photorefractive crystal is centered in the lens axis and the lens position is adjusted for maximum output from the lock-in amplifier. The objective lens F-number is 2, the lens back aperture diameter is $\approx$25 mm, the target-plate-to-lens input principal plane distance is $\approx$238 mm, and the lens focus is 50 mm, which result in a 0.27 lens magnification of the target lateral movement and an average speckle radius $R_0 \approx 3.3$ μm. This estimated R_0 value assumes uniform lens illumination and diffraction limited conditions and is therefore a minimum limit speckle size value. The use of a lens produces a much larger signal than that from a delocalized speckle pattern without the lens. The delocalized speckle would directly translate the transverse target movement onto the crystal, whereas the lens produces a deamplification in the imaging process as computed above. However, the lens reduces the speckle size in the image plane so that the vibration amplitude deamplification is roughly compensated for. The advantage of the focusing lens simply stems from the much larger amount of scattered light collected onto the CdTe crystal.

The i^{Ω} for a fixed irradiance $I \approx 1.16$ mW/cm^2 measured behind the crystal [with the irradiance at the input plane inside the crystal being $I(0) \approx 3I = 3.48$ mW/cm^2] and different frequencies Ω are reported in Fig. 5. Here we see that for the higher frequencies, where the $\Omega\tau_{SC} \gg 1$ condition is approximately fulfilled, a maximum in i^{Ω} is observed at $\delta \approx 0.9$, which is in good agreement with theory. For the lower frequencies, this maximum does not show up, as expected, because the photorefractive space-charge buildup time is comparatively fast compared to the vibration period. Independent experiments have shown that, for the irradiance in this experiments [$I(0) \approx 3.48$ mW/cm^2], the response time of our sample is approximately 3.6 ms at the input plane.

IV. DISCUSSION AND CONCLUSIONS

The present paper describes a more realistic mathematical model than ever reported before about speckle photo-emf effects for relatively large vibration amplitudes and represents a considerable improvement over a previously reported[13] one. This model reports, for sufficiently fast vibrations, the presence of a maximum in the first harmonic photo-emf signal term $i^{\Omega} \propto b_1$ at a fixed value of δ that varies between 0.85 (for $R_d = 0.1$) and 0.9 (for $R_d = 0$), and this value does apparently depend on the dark-to-photoconductivity ratio R_d only. The position of this maximum could be used as a reference point for calibrating the setup. The preliminary experimental results reported here for CdTe:V are in good agreement with theory.

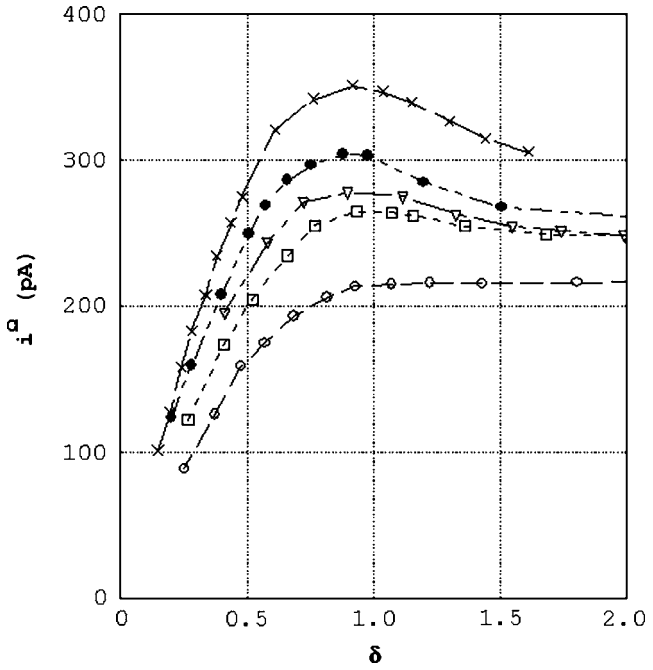

FIG. 5. First harmonic photocurrent $i^{\Omega} \propto b_1$ measured in CdTe:V as a function of δ for $\Omega/2\pi = 200$ Hz (○), 400 Hz (□), 615 Hz (▽), 1300 Hz (●), and 1700 Hz (×), always at $I(0) \approx 3.48$ mW/cm^2.

The present results may open interesting perspectives for the practical application of photo-emf to transverse vibration amplitude measurement and for further exploration of the different relations among the many experimental parameters involved. Although CdTe is a rather fast response material that is better suited for ultrasonic than audio-range vibration measurement, the low light irradiances involved here do increase the material response time enough to enable the measurement of vibrations in the 1–2 kHz range too.

ACKNOWLEDGMENTS

We strongly acknowledge the Conselho Nacional de desenvolvimento Científico e tecnológico (CNPq) as well as the Fundação de amparo à Pesquisa do Estado de São Paulo (FAPESP) for their financial support. We also acknowledge Professor Paulo H. Sakanaka from IFGW/UNICAMP, Brazil, for his help with the MATHEMATICA software for calculations and Professor S.G. Odoulov from the Institute of Physics, National Academy of Sciences, Kiev, Ukraine, for his useful suggestions.

[1] I. A. Sokolov and S. I. Stepanov, Electron. Lett. **26**, 1275 (1990).
[2] N. Noginova, N. Kukhtarev, M. Noginov, B. Chen, H. Caulfield, and P. Venkateswarlu, J. Opt. Soc. Am. B **13**, 2622 (1996).
[3] G. S. Trofimov and S. I. Stepanov, Sov. Phys. Solid State **28**, 1559 (1986).
[4] N. A. Korneev and S. I. Stepanov, J. Mod. Opt. **38**, 2153 (1991).
[5] I. A. Sokolov and S. I. Stepanov, Appl. Opt. **32**, 1958 (1993).
[6] S. I. Stepanov, in *Semiconductor Devices*, edited by H. S. Nalwa, Handbook of Advanced Electronic and Photonic Materials and Devices Vol. 2 (Academic, New York, 2001), Chap. 6, pp. 205–272.
[7] J. Castillo, P. Rodriguez, A. Aguirre, S. Stepanov, and S. Mansurova, Appl. Phys. Lett. **80**, 3697 (2002).
[8] I. A. Sokolov and S. I. Stepanov, J. Opt. Soc. Am. B **10**, 1483 (1993).

[9]P. Rodriguez, S. Trivedi, F. Jin, C.-C. Wang, S. Stepanov, J. F. Meyers, J. Lee, and J. Khurgin, Appl. Phys. Lett. **83**, 1893 (2003).
[10]S. Stepanov, P. Rodriguez, S. Trivedi, and C.-C. Wang, Appl. Phys. Lett. **84**, 446 (2004).
[11]N. Korneev and S. Stepanov, Opt. Commun. **115**, 35 (1995).
[12]L. Mosquera and J. Frejlich, J. Opt. Soc. Am. B **19**, 2904 (2002).
[13]L. Mosquera and J. Frejlich, J. Opt. A, Pure Appl. Opt. **6**, 1001 (2004).
[14]S. Stepanov, I. Sokolov, G. Trofimov, V. Vlad, D. Popa, and I. Apostol, Opt. Lett. **15**, 1239 (1990).
[15]N. A. Korneev and S. Stepanov, J. Appl. Phys. **74**, 2736 (1993).
[16]P. Heinz and E. Gamire, Appl. Phys. Lett. **84**, 3196 (2004).
[17]C.-C. Wang, S. Trivedi, F. Jin, K. Jia, H. He, G. Elliott, and J. Khurgin, J. Opt. Soc. Am. B **19**, 177 (2002).
[18]S. I. Stepanov, P. Rodríguez, S. Mansurova, M. L. Arroyo, S. Trivedi, and C. C. Wang, Opt. Mater. (Amsterdam, Neth.) **29**, 623 (2007).
[19]Y. Gnatenko, M. Brodyn, I. Faryna, P. Bukivskij, O. Shigiltchoff, M. Furyer, R. Gamernyk, N. Kukhtarev, and T. Kukhtareva, Phys. Status Solidi A **204**, 2431 (2007).
[20]M. Gather, S. Mansurova, and K. Meerholz, Phys. Rev. B **75**, 165203 (2007).
[21]F. A. Jenkins and H. E. White, *Fundamentals of Optics*, 4th ed. (McGraw-Hill, Auckland, 1981).
[22]Y. Marfaing, J. Cryst. Growth **197**, 707 (1999).
[23]P. Günter and J. P. Huignard, *Photorefractive Materials and Their Applications I* Topics in Applied Physics Vol. 61, edited by P. Günter and J.-P. Huignard (Springer-Verlag, Berlin, 1988).
[24]J. Frejlich, *Photorefractive Materials: Fundamental Concepts, Holographic Recording, and Materials Characterization* (Wiley-Interscience, New York, 2006).